Evaluation of NOAA-20 VIIRS Reflective Solar Bands Early On-Orbit Performance Using Daily Deep Convective Clouds Recent Improvements

Wenhui Wang and Changyong Cao

***Abstract*—The visible infrared imaging radiometer suite (VIIRS) onboard the National Oceanic and Atmospheric Administration - 20 (NOAA-20) satellite was successfully launched in November 2017. During the NOAA-20 VIIRS postlaunch test [(PLT) or extensive cal/val, launch—April 30, 2018], a daily deep convective cloud (DCC) method was developed to support the timely decision making of reflective solar bands (RSBs) on-orbit calibration updates. Different from its predecessor, the VIIRS onboard the Suomi National Polar-Orbiting Partnership (S-NPP) satellite, NOAA-20 VIIRS RSBs have been calibrated using constant calibration factors since April 27, 2018, with the assumption that no significant instrument responsivity change occurs. In this study, the daily DCC method was further refined for evaluating NOAA-20 VIIRS RSB performance after two years on-orbit. An annual cycle climatology for DCC was developed to reduce uncertainty in the trend analysis. NOAA-20 VIIRS observations during the PLT were reprocessed to generate consistent data records. Two-year trends (January 6, 2018–January 5, 2020) were analyzed using consolidated (reprocessed + operational) NOAA-20 daily DCC time series and compared with S-NPP. NOAA-20 daily DCC time series for the visible and near-infrared bands shows small upward trends (up to 0.4%/year in M1), while no significant trend was observed in S-NPP. Moreover, NOAA-20 *I*3 and M10 exhibit larger than the expected interchannel inconsistency (∼1.2%) compared with S-NPP. NOAA-20 RSBs are biased ∼1.5%–4.5% lower than S-NPP, generally consistent with results from other methods.**

***Index Terms*—Calibration biases and trends, daily deep convective clouds (DCCs), National Oceanic and Atmospheric Administration – 20 (NOAA-20), reflective solar bands (RSBs), Suomi National Polar-Orbiting Partnership (S-NPP), visible infrared imaging radiometer suite (VIIRS).**

I. Introduction

THE visible infrared imaging radiometer suite (VIIRS) onboard the National Oceanic and Atmospheric Administration - 20 (NOAA-20) satellite was launched on November 18, 2017, following six years of successful operations of its predecessor on the Suomi National Polar-Orbiting Partnership (S-NPP) satellite [1]–[3]. Both S-NPP and NOAA-20 VIIRS instruments are equipped with five imaging bands (*I*-bands), 16 moderate-resolution bands (*M*-bands), and one day/night band. NOAA-20 VIIRS sensor data records (SDR) achieved beta, provisional, and validated maturity statuses on February 1, February 19, and April 30, 2018, respectively. The operational NOAA-20 VIIRS SDR products are available to the public through the NOAA comprehensive large array-data stewardship system since February 1, 2018. Similar to S-NPP, NOAA-20 VIIRS SDR products are valuable for monitoring severe weather events and air quality, and for deriving a wide variety of environmental data records (EDR), such as cloud and aerosol properties, ocean color, sea/land/ice surface temperature, active fires, and earth's albedo.

Two years of NOAA-20 VIIRS SDRs are available up-to-date. NOAA-20 operates in the same orbital plane as S-NPP, with NOAA-20 ∼50 min (half orbit) ahead of S-NPP. NOAA-20 VIIRS observations, together with those from S-NPP VIIRS, enable users to develop blended EDR products with fewer data gaps and/or improved temporal resolution. It is important to characterize the on-orbit calibration performance of the NOAA-20 VIIRS to support user communities.

Deep convective clouds (DCCs) are stable targets for the on-orbit calibration stability monitoring of satellite radiometers in the solar reflective spectrum [4]–[8]. Monthly/semimonthly DCC time series have been used for S-NPP VIIRS reflective solar bands (RSBs) long-term calibration stability monitoring [6]–[8]. However, the monthly DCC method, as well as other vicarious methods, cannot provide reliable results in a timely manner during the VIIRS postlaunch test [(PLT), or intensive cal/val] period, when frequent on-orbit calibration updates are made to transfer calibration from prelaunch to postlaunch and to further refine on-orbit calibration. As an improvement, daily DCC time series were introduced in early 2018 to monitor NOAA-20 VIIRS RSB calibration and support the timely decision making of on-orbit calibration updates [9], [10]. Gong *et al.* [11] explored the feasibility of using daily and weekly DCC time series to monitor the S-NPP VIIRS RSB calibration stability and found that the degradation trends derived using the daily and weekly DCC time series are consistent with that from the monthly DCC time series. Moreover, a short-term calibration anomaly that lasts much shorter than a month, therefore, usually overlooked by monthly DCC time series can be successfully detected.

Manuscript received February 28, 2020; revised May 17, 2020 and June 11, 2020; accepted July 5, 2020. Date of publication July 7, 2020; date of current version July 22, 2020. This work was supported by NOAA under Grant NA19NES4320002 (Cooperative Institute for Satellite Earth System Studies) at the University of Maryland/ESSIC. *(Corresponding author: Wenhui Wang.)*

Wenhui Wang is with CISESS/ESSIC, the University of Maryland, College Park, MD 20742 USA (e-mail: wenhui.wang@noaa.gov).

Changyong Cao is with NOAA/Center for Satellite Applications and Research, College Park, MD 20740 USA (e-mail: changyong.cao@noaa.gov).

Digital Object Identifier 10.1109/JSTARS.2020.3007863

TABLE I
SPATIAL AND SPECTRAL CHARACTERISTICS OF NOAA-20 AND S-NPP VIIRS RSBS

		Spatial Resolution at nadir (m)	Center Wavelength (μm)		Gain	Ltyp	Lmin	Lmax
			S-NPP	NOAA-20				
VISNIR	M1	750	0.411	0.412	H L	44.9 155	30	135 615
	M2	750	0.444	0.445	H L	40 146	26	127 687
	M3	750	0.486	0.489	H L	32 123	22	107 702
	M4	750	0.551	0.557	H L	21 90	12	78 667
	I1	375	0.639	0.644	S	22	22	718
	M5	750	0.672	0.667	H L	10 68	9	59 651
	M6	750	0.745	0.746	S	9.6	5.3	41
	I2	375	0.862	0.867	S	25	25	349
	M7	750	0.862	0.868	H L	6.4 33.4	3.4	29 349
SWIR	M8	750	1.238	1.238	S	5.4	3.5	165
	M9	750	1.375	1.375	S	6	0.6	77.1
	I3	375	1.602	1.604	S	7.3	7.3	72.5
	M10	750	1.602	1.605	S	7.3	1.2	71.2
	M11	750	2.257	2.258	S	0.12(NPP) 0.1 (NOAA-20)	31.8	10

The unit of Ltyp (typical radiance), Lmin (minimum radiance), and Lmax (maximum radiance) is W/(m^2 μm sr). *M*1–*M*5 and *M*7 are the dual gain bands: *H* (high gain) and *L* (low gain); *I*1–*I*3, *M*6, and *M*8–*M*11 are the single gain bands (S).

The purpose of this study is to analyze NOAA-20 VIIRS RSB two-year on-orbit calibration performance using the daily DCC method. In this study, the daily and monthly DCC methods for VIIRS were refined to reduce the uncertainty caused by annual variations in DCC reflectance. The characteristics of daily DCC time series were analyzed in depth. NOAA-20 VIIRS SDRs from the early mission were reprocessed. Two-year trends were derived using consolidated (reprocessed and operational) SDRs and compared with that of S-NPP. The methodology developed in this study can also be applied to the VIIRS onboard the future joint polar satellite system (JPSS) satellites and other radiometers.

The rest of this article is organized as follows. The NOAA operational and reprocessed SDRs for NOAA-20 and S-NPP VIIRS used in this study are described in Section II. Section III presents the daily DCC method. Section IV focuses on the characteristics of the daily DCC time series. Section V presents the NOAA-20 VIIRS RSB early on-orbit performance. Section VI summarizes this study.

II. DATA

A. NOAA Operational VIIRS SDRs for NOAA-20 and S-NPP

NOAA-20 VIIRS nadir door was opened on December 13, and NOAA operational RSB SDRs became available on December 20, 2017. NOAA-20 cryoradiator door was opened on January 3, 2018, and the 11 μm band *M*15) required for DCC detection became available after cold focal plane assemblies reached nominal temperature on January 5, 2018, around 8:30 UTC. Two years of NOAA operational NOAA-20 VIIRS radiance SDRs and geolocation products from January 6, 2018, to January 5, 2020, were used in this study. NOAA operational S-NPP VIIRS SDRs during the same period were also used for the comparison purpose.

VIIRS has 14 RSBs (*I*1–*I*3 and *M*1–*M*11), covering a spectral range from $\sim$0.4 to 2.3 μm. Table I summarizes the spatial and spectral characteristics of NOAA-20 and S-NPP VIIRS RSB bands evaluated in this study. Note that the VIIRS *M*1–*M*5 and *M*7 are the dual gain bands. DCCs are very bright at the visible and near-infrared (VIS/NIR) spectrum. For these bands, only the calibration at low gain was evaluated using DCCs. *M*6 saturated over DCCs; therefore, it is not considered here.

The on-orbit calibration of NOAA operational S-NPP VIIRS RSBs has relied on an automated calibration procedure (RSBAutoCal) since December 2015, with on-orbit calibration factors (*F*-factor) updated per orbit, i.e., 14$\times$ per day [12], [13]. The calibration of S-NPP RSBs during the study period has been stable based on our monitoring results, except for two short-term anomalies: First, *M*4/*M*5 calibration anomaly due to the missing of calibration data (February 19–25, 2018), and second solar diffuser (SD) digital count change, starting from February 24, 2019. The calibration of VIS/NIR bands was recovered about one month later by the RSBAutoCal SD degradation factor (*H*-factor) update. However, the anomaly in the short-wave infrared (SWIR) bands has not to be resolved up-to-date.

Different from S-NPP, NOAA-20 RSBs have been calibrated so far without automation, with automated calibration still subject to further analysis and tuning. Four on-orbit RSB

TABLE II
NOAA-20 VIIRS RSB OPERATIONAL ON-ORBIT CALIBRATION UPDATES

	Time	Bands Affected
1	1/5/2018	M1-M7, I1-I2
2	2/6/2018	M1-M11, I1-I3
3	3/23/2018	M1-M7
4	4/27/2018	M1-M7

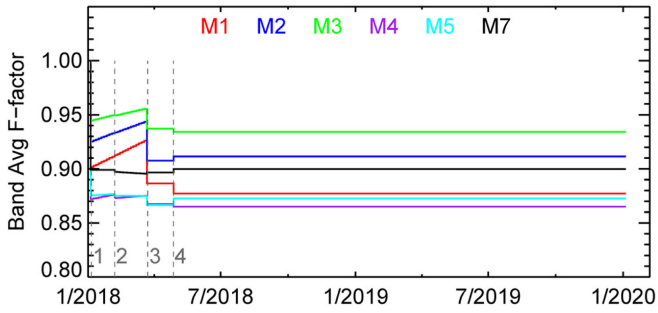

Fig. 1. NOAA-20 VIIRS *M*1–*M*5 and *M*7 band-averaged *F*-factors (low gain) used in the NOAA operational processing.

F-factor updates (see Table II) have been implemented in the operational processing to transfer calibration from prelaunch to on-orbit and to further improve the on-orbit calibration. Fig. 1 shows the band-averaged *F*-factors for *M*1–*M*5 and *M*7 low gain. Note that VIIRS RSB high-gain *F*-factors are similar to that of low gain for the dual gain bands. NOAA-20 VIIRS RSBs have been calibrated using constant *F*-factors since the latest on-orbit update on April 27, 2018.

The calibrations of NOAA-20 and S-NPP *M*15 were monitored using colocated cross-track infrared sunder (CrIS) observations [10]. Our results show that the on-orbit calibrations of NOAA-20 and S-NPP VIIRS *M*15 brightness temperatures (BTs) are stable during the study period. In this study, we further analyzed the two-year stability of VIIRS-CrIS BT biases at 205 K scene temperature and locations (near nadir) used for DCC detection. The results show that VIIRS agrees with CrIS ~0.45 K (S-NPP) and ~0.5 K (NOAA-20). Small but similar seasonal variations (~±0.1 K) were observed in the *M*15 VIIRS-CrIS BT bias time series at 205 K scene temperature for both NOAA-20 and S-NPP. The seasonal variation may be due to the insufficient data samples during fall/winter months (ten times smaller than that in spring/summer months). The seasonable variations may contribute to the annual cycles in the DCC time series when the mean of DCC reflectance is used. This topic will be further discussed in Section III-B. NOAA-20 and S-NPP VIIRS geolocation errors are within 200 m during the entire study period.

B. NOAA STAR Reprocessed S-NPP VIIRS SDRs

S-NPP VIIRS SDRs from January 2012 to March 2017 have been reprocessed at the NOAA Center of Satellite Research and Applications (STAR) using the latest algorithms and calibration parameters. During the reprocessing, RSB baseline SDRs were calibrated using the improved RSBAutoCal *F*-factors. The annual oscillations in the RSBAutoCal *F*-factors were removed based on the reanalyzed SD and SD stability monitor screen and the bidirectional reflectance distribution function parameters. In addition, *F*-factors were further smoothed to reduce spurious spikes. Our analyses indicate that the reprocessed RSB baseline SDRs, as well as *M*15 BT and geolocation products, are stable from January 1, 2013, to December 31, 2016. These four years of data were used to characterize and correct annual cycles in the DCC time series (see Section III-B). The S-NPP reprocessed VIIRS SDRs are available to download online at [14].

C. Reprocessed NOAA-20 VIIRS SDRs

To address the calibration inconsistencies in the early mission data, NOAA-20 VIIRS SDRs from December 13, 2017, to April 30, 2018, were reprocessed using consistent calibration parameters. During the reprocessing, constant *F*-factors, which have been used in the NOAA operational processing since April 27, 2018, were used for RSB calibration. In this study, the daily DCC time series generated using the reprocessed SDRs were consolidated with those using the operational SDRs after May 1, 2018. Two-year trends were analyzed using the consolidated daily DCC time series to characterize NOAA-20 VIIRS RSB on-orbit instrument responsivity change (see Section V).

III. METHODOLOGY

A. Daily and Monthly DCC Methods for VIIRS

In this study, VIIRS DCC pixels were identified based on the following criteria:

1) *M*15 (11 μm) BT (TB11) $<=$ 205 K;
2) the standard deviation of TB11 of the subject pixel and its eight adjacent pixels $<=$ 1 K;
3) the standard deviation of RSB reflectance of the subject pixel and its eight adjacent pixels $<=$ 3%;
4) the solar zenith angle $<=$ 40°;
5) the view zenith angle $<=$ 35° (to avoid the bow-tie effect in VIIRS SDRs).

Similar criteria were used in previous studies [4], [7], [8]. Moreover, DCCs over the entire intertropical convergence zone with latitude within ±25° were used to maximize the sample size for more reliable results. On average, ~330 000 DCC pixels (for *M*-bands) are available daily. To reduce the daily noise in the DCC time series, days with less than 1 00 000 DCC pixels were excluded when the daily DCC method is used.

The anisotropic effects in the VIIRS VIS/NIR bands (*M*1–*M*5, *M*7, and *I*1 and *I*2) were corrected using a 0.65 μm angular distribution model (ADM) developed by Hu *et al*. in 2004 (HU2004) [4]. This HU2004 ADM performs well in bands with center wavelength closer to 0.65 μm, such as VIIRS bands *M*5 and *M*7. However, the HU2004 ADM model was not applied to the VIIRS SWIR bands (*M*8–*M*11 and *I*3) due to the fact that the anisotropic effects in the bands are different [4], [6], [8], [15]. The seasonal variations were observed in the DCC time series for SWIR bands (without the anisotropic effect correction) as well as in the shorter wavelength VIS/NIR bands

(after the anisotropic effect correction). To address this issue, a DCC seasonal cycle climatology was developed with four years of reprocessed S-NPP VIIRS SDRs and used to reduce the seasonal cycles in the daily and monthly DCC time series (see Sections II-B and III-B).

The mean and mode of daily and monthly DCC statistics (mean and mode) were calculated and used for characterizing the VIIRS RSB responsivity change, interchannel, and intersatellite biases. Similar to previous studies using the monthly DCC method [4], [6], [8], and [15], the mode of daily DCC reflectance was used for VIS/NIR individual bands calibration assessment, while the mean of daily DCC reflectance was used for the assessment of SWIR individual bands. The mean of DCC reflectance was also used for band ratios for the interchannel and intersatellite comparisons. The spectral differences between NOAA-20 and S-NPP VIIRS (see Table I) were corrected using the spectral band adjustment factors (SBAF), which are computed from algorithms and online tools developed at NASA-LaRC with the scanning imaging absorption spectrometer for atmospheric chartography (SCIAMACHY) V7.01 data obtained from the European Space Agency Envisat Program [16], [17].

In this study, the linear trends of daily and monthly DCC time series were used to quantify calibration stability and degradation trends for each band. Linear trend (b_1) and intercept (b_0) were calculated using the ordinary least square method. Uncertainty and 95% confidence interval (CI) for the linear trend was derived using a method given in [18]

$$\sigma_b = \sqrt{\hat{\sigma}^2 / S_{xx}} \tag{1}$$

$$S_{xx} = \sum_{i=1}^{n} (x_i - \bar{x})^2 \tag{2}$$

$$\hat{\sigma}^2 = \frac{\sum_{i=1}^{n} (y_i - y_{i,\text{fitted}})^2}{n-2} \tag{3}$$

where σ_b is the uncertainty for the linear trend, n is the number of data samples, x_i is the time, $\bar{x}$ is the mean value of time, y_i is the daily or monthly DCC reflectance, $y_{i,\text{fitted}} = b_0 + b_1 \cdot x_i$ is the linear model predicted daily or monthly DCC reflectance, and $\hat{\sigma}^2$ is the variance of error term ($\varepsilon_i = y_i - y_{i,\text{fitted}}$) with n-2 degree of freedom (two degrees of freedom have already been used for calculating b_0 and b_1). It is assumed that the error term is normally and independently distributed. CI for the linear trend is estimated as

$$\text{CI} = b_1 \pm t_{\alpha/2,\, n-2} \cdot \sigma_b \tag{4}$$

where $t_{\alpha/2,n-2}$ is the one-tailed probability that a random variable from the student's t distribution, with $n-2$ degree of freedom, is less or equal than $\alpha/2$ ($\alpha = 0.05$ for the 95% CI). For the 95% CI and $n-2> = 6$, $t_{0.025,n-2}$ is very close to two. A linear trend is significantly different from zero if the 95% CI for the trend does not cross zero.

B. Correction of Annual Cycles in the DCC Time Series

The seasonal variations were observed in the DCC time series in the SWIR bands (without ADM correction) and in some VIS/NIR bands (with ADM correction). While the seasonal cycle has little impact on long-term trends analysis (when several years of data are available) and the detection of large calibration changes, it compromises the ability to use the DCC method to detect smaller calibration changes and to characterize early on-orbit instrument responsivity trends when the available data record is still short.

In this study, annual cycles in the VIIRS RSBs DCC time series were estimated using four years (2013–2016) of reprocessed S-NPP VIIRS SDRs (see Section II-B). The monthly DCC time series were generated using the method given in Section III-A. The anisotropic effect in the VIS/NIR bands was corrected using the HU2004 ADM before the estimation of annual cycle climatology. For each band, the DCC annual cycle climatology for the mean and mode of DCC reflectance was estimated using monthly DCC reflectance anomalies, i.e., monthly DCC reflectance minus four years averaged DCC reflectance.

Fig. 2(a)–(c) shows the examples of DCC annual cycle climatology for *M*2, *M*7, and *M*8. The monthly DCC time series before and after the correction of annual cycles were shown in Fig. 2(d)–(f). Annual cycles in the mean DCC time series are larger than that of the mode DCC time series. Due to the fact that the HU2004 ADM is not effective for SWIR bands, the annual cycles in SWIR bands estimated here are usually larger than in the VIS/NIR bands. For the monthly DCC time series, the annual cycle climatology can be used directly. For the daily DCC time series, the correction term is interpolated using the monthly annual cycle climatology.

The annual cycles in the S-NPP and NOAA-20 DCC time series are expected to be very close to each other. NOAA-20 and S-NPP VIIRS operate on the same orbital plane with similar local equator crossing time. NOAA-20 VIIRS spectral response functions match well with that S-NPP. The same DCC detection criteria and the ADM correction method were used for the two VIIRS. For the SWIR bands, the annual cycle climatology is dominated by the DCC anisotropic effect. For the VIS/NIR bands, the annual cycle climatology is dominated by the residual anisotropic effect after the HU2004 ADM correction.

We analyzed the impacts of other factors on the annual cycle climatology developed using the reprocessed S-NPP data:

1) The seasonal variations of the errors in the S-NPP RSB prelaunch calibration coefficients.
2) The spurious seasonal variations in the S-NPP RSB on-orbit *F*-factors.
3) The seasonal variations of errors in *M*15 BTs at 205 K scene temperature and near nadir locations.

S-NPP prelaunch calibration coefficients were carefully characterized at different instrument temperature plateaus using the National Institute of Standards and Technology traceable calibration sources. During the S-NPP reprocessing, the optimal versions of prelaunch calibration coefficients were used. Moreover, the spurious seasonal variations in the RSB *F*-factors were carefully analyzed and removed. Our evaluation results indicate that the reprocessed S-NPP RSB baseline SDRs were stable from 2013 to 2016. Therefore, we assume that the impact of the calibration errors in the S-NPP reprocessed SDRs on the annual cycle climatology is small. We also analyzed the seasonal variations of NOAA-20 and S-NPP *M*15 near nadir BTs

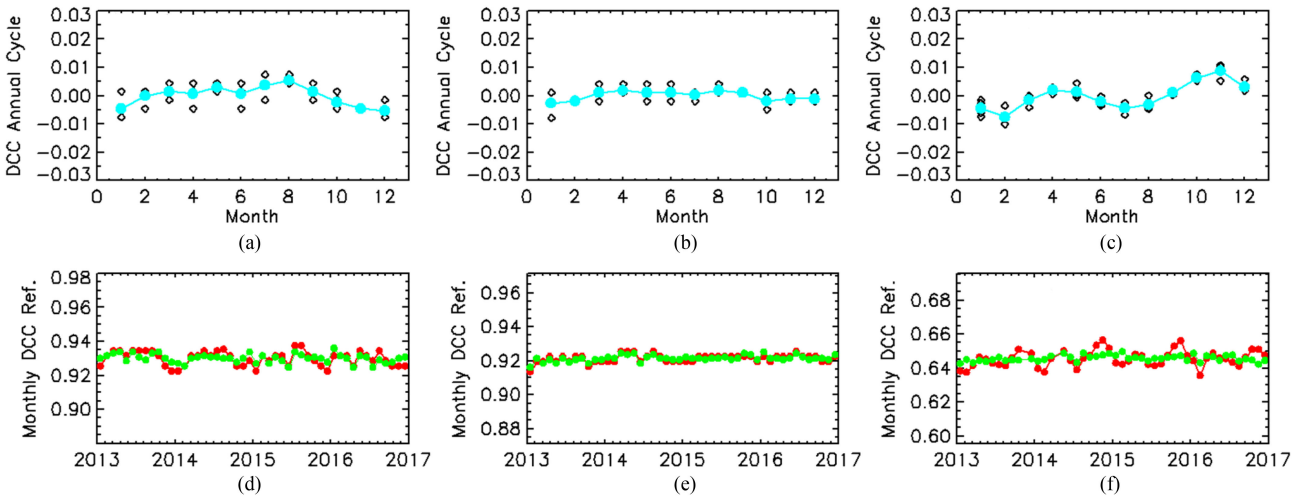

Fig. 2. Top panel: VIIRS DCC annual cycle climatology (cyan color) estimated using four years (2013–2016) of S-NPP VIIRS reprocessed baseline SDRs for (a) M2 mode, (b) M7 mode, and (c) M8 mean. The open black circles are the mode or mean of DCC reflectance for individual months. Bottom panel: S-NPP (a) M2 mode, (b) M7 mode, (c) M8 mean monthly DCC time series before (red color) and after (green color) the correction of annual cycles.

TABLE III
COMPARISON OF NOAA-20 RSB DAILY AND MONTHLY DCC TIME SERIES BEFORE AND AFTER THE ANNUAL CYCLE CORRECTION

		Before Annual Cycle Correction(Daily/Monthly)			After Annual Cycle Correction(Daily/Monthly)		
		Avg. DCC Ref. (%)	StdDev (%)	Trend ± 95%CI	Avg. DCC Ref.	StdDev (%)	Trend ± 95%CI
VIS/NIR	M1	0.914/0.916	1.1/0.5	0.1±0.2/-0.0±0.5	0.914/0.916	1.0/0.3	0.3±0.2/0.2±0.3
	M2	0.911/0.914	1.1/0.5	0.1±0.2/-0.1±0.5	0.911/0.914	1.1/0.2	0.3±0.2/0.3±0.2
	M3	0.904/0.906	1.1/0.5	0.0±0.2/-0.0±0.5	0.904/0.906	1.1/0.2	0.3±0.2/0.2±0.2
	M4	0.868/0.870	1.1/0.5	0.1±0.2/-0.1±0.5	0.868/0.870	1.1/0.3	0.2±0.2/0.1±0.3
	M5	0.892/0.894	1.0/0.5	0.0±0.2/-0.1±0.5	0.892/0.894	1.0/0.2	0.2±0.2/0.1±0.2
	M7	0.886/0.887	0.8/0.3	0.1±0.1/-0.0±0.3	0.886/0.887	0.8/0.2	0.2±0.1/0.0±0.2
	I1	0.868/0.870	1.0/0.3	0.1±0.2/0.1±0.3	0.868/0.870	1.0/0.2	0.3±0.2/0.2±0.2
	I2	0.882/0.883	0.7/0.2	0.1±0.1/0.0±0.2	0.882/0.883	0.7/0.2	0.2±0.1/0.1±0.2
SWIR	M8	0.631/0.631	1.4/0.8	0.6±0.2/0.6±0.8	0.631/0.630	1.2/0.4	0.3±0.2/0.3±0.4
	M9	0.565/0.654	2.6/1.5	1.1±0.4/1.1±1.5	0.564/0.564	2.3/0.7	0.8±0.4/0.7±0.7
	M10	0.211/0.210	3.3/2.2	1.7±0.5/1.7±2.2	0.210/0.210	2.5/0.8	0.8±0.4/0.7±0.8
	M11	0.336/0.335	2.6/1.7	1.2±0.4/1.3±1.7	0.335/0.335	2.0/0.6	0.5±0.3/0.5±0.6
	I3	0.208/0.208	3.3/2.2	1.7±0.5/1.7±2.2	0.208/0.208	2.6/0.8	0.8±0.4/0.7±0.8

Averaged DCC reflectance, standard deviation (StdDev, %), trend (%/year), and 95% confidence interval (CI) for the trend were calculated using data from May 1, 2018, to December 31, 2019.

at 205 K scene temperatures using colocated CrIS observations. The results show that NOAA-20 and S-NPP exhibit similar small seasonal variations (both $\sim\pm 0.1$ K). The mode and mean of DCC reflectance are not sensitive to $M15$ BT bias on the order of 0.5 K, especially when the mode of DCC reflectance is used [7]. Overall, the impacts of the three factors on NOAA-20 degradation trend analysis will be very small when the S-NPP annual cycle climatology is applied to NOAA-20. The effectiveness of correcting NOAA-20 DCC annual cycles using the S-NPP annual cycle climatology will be verified in Section IV-A.

IV. CHARACTERISTICS OF VIIRS DAILY DCC TIME SERIES

A. Comparison of Daily and Monthly DCC Time Series

We compared NOAA-20 S-NPP daily and monthly DCC time series before and after the annual cycle correction. The statistics of daily and monthly DCC time series for all NOAA-20 RSBs are summarized in Table III. The averaged DCC reflectance, standard deviation, trend, and the 95% CI for the trend were calculated using the data from May 1, 2018, to December 31, 2019, after the latest on-orbit calibration update and NOAA-20 archived the validated maturity status. The standard deviation was calculated after removing the linear trend in the time series to quantify the variability of DCC reflectance with the absence of instrument response degradation. Note that the trends given in Table III are used for comparing the daily and monthly DCC methods only, instead of studying NOAA-20 RSB sensor response degradation, which will be analyzed in Section V using longer data records. The similarities and differences between the S-NPP daily and monthly DCC time series are comparable with that of NOAA-20.

Fig. 3 compares NOAA-20 daily and monthly DCC time series for representative VIS/NIR bands. It can be observed that the annual variations in the $M1$ and $M4$ DCC time series are effectively reduced after applying the annual cycle correction. Similar results are observed in bands $M2$ and $M3$. The impacts

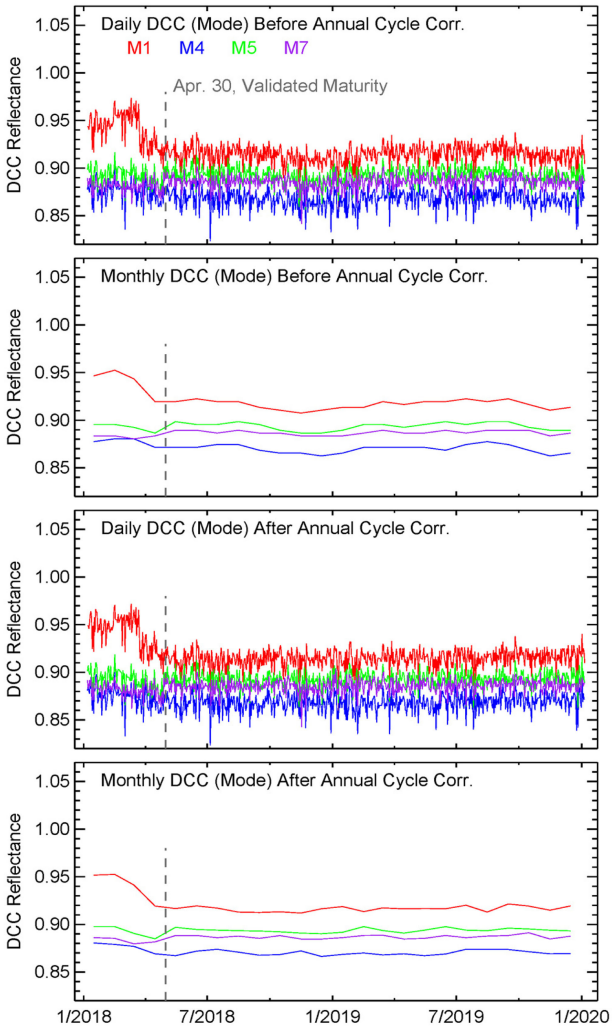

Fig. 3. Comparison of NOAA-20 *M*1, *M*4, *M*5, and *M*7 daily and monthly DCC time series.

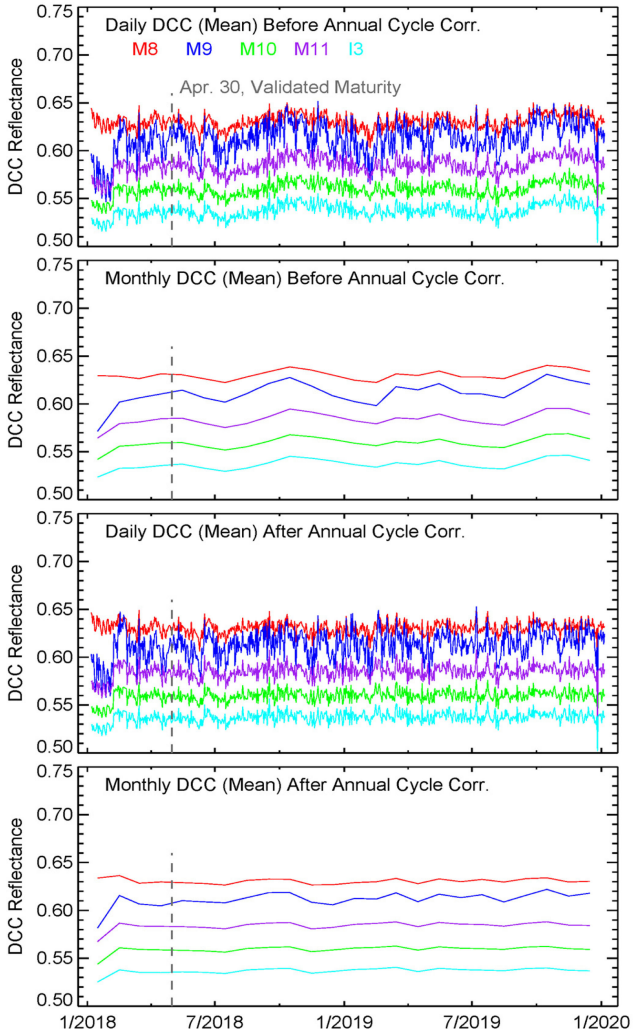

Fig. 4. Comparison of NOAA-20 daily and monthly DCC time series for SWIR bands.

of the annual cycle correction on *M*5, *M*7, and *I*1 and *I*2 are smaller than on *M*1–*M*4 because the HU2004 ADM correction performs well for these bands. The averaged DCC reflectance and trends estimated using the daily and monthly DCC time series match well with each other. The averaged DCC reflectance agrees within 0.2% in most cases. The trends agree within 0.1%/year for the majority of bands (within 0.2% for all cases). A similar consistency was observed for all VIS/NIR bands. However, trends estimated using time series before and after annual correction are about 0.1%–0.2% different because only 1.5 years of data were used.

With standard deviations range from 0.7% to 1.1%, VIS/NIR daily DCC time series after the correction of annual cycles are noisier than the monthly DCC time series (0.2%–0.3%). Moreover, the variability of daily DCC reflectance is dominated by the limited number of DCC pixels available each day. Applying annual cycle correction has no significant impact on the noise level. Moreover, varying the step size used for calculating the mode of daily DCC reflectance does not change the results significantly, consistent with Gong et al. [11].

Although VIS/NIR daily DCC time series are noisier, they have a much higher temporal resolution. In addition, the annual cycle correction applied in this study also slightly reduces the uncertain of the daily DCC method. The 95% CI for the trends indicates that the uncertainties in the trends derived using the daily DCC method are comparable or smaller than those of the monthly DCC method for the VIS/NIR bands (see Table III, after the annual cycle correction).

Fig. 4 compares NOAA-20 daily and month DCC time series for the SWIR bands. The band-dependent constant offsets were added for *M*9–*M*11 and *I*3 to better illustrate the time series. The statistics of the daily and monthly DCC time series for the SWIR bands are summarized in Table III. Similar to the VIS/NIR bands, the averaged DCC reflectance and trends estimated using the two DCC methods also agree well with each other, within 0.1% in the majority of cases. The absolute noises in the SWIR and VIS/NIR daily DCC time series are similar, except for *M*9 (noisier than the other bands). Due to the fact that DCCs are less reflective in the SWIR spectrum, the relative noises (after divided by averaged DCC reflectance and converted to a percentage, see

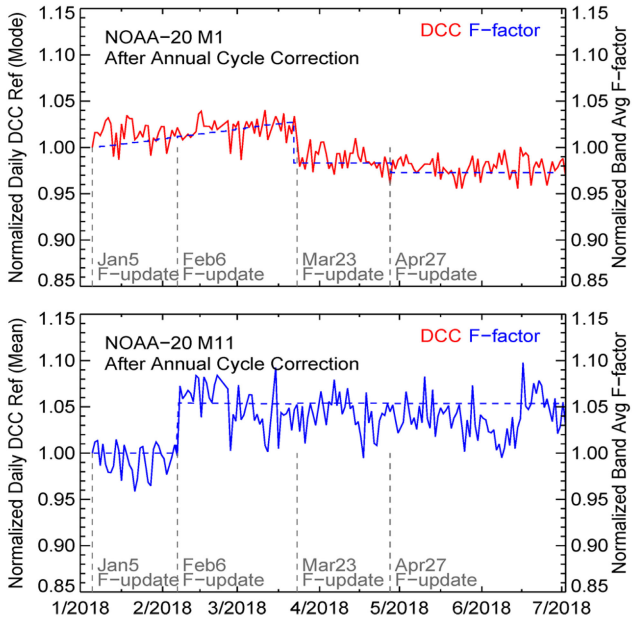

Fig. 5. Comparison of NOAA-20 daily DCC reflectance and band-averaged *F*-factor (low gain) time series for *M*1 (top) and *M*11 (bottom).

Table III) in the SWIR bands are larger than that of VIS/NIR bands.

The annual cycle correction has larger impacts on the SWIR bands compared with the VIS/NIR bands due to the fact that no ADM correction was applied to these bands. After the correction, the annual variations in the time series are significantly reduced. The trends derived using the data before and after the annual cycle correction can differ more than 100%. The uncertainties in the trends derived using the daily DCC method are only about 50% of that of the monthly DCC method due to the increased temporal sampling frequency.

B. Sensitivity of the Daily DCC Time Series to Calibration Change

Four NOAA-20 RSB on-orbit calibration updates have been performed in the operational processing during the NOAA-20 PLT period (see Table I). Unlike the unexpected calibration anomalies, the changes of *F*-factors are well known before and after these planned events. Therefore, they provided valuable opportunities to verify the effectiveness of using the daily DCC method to support the timely decision making of operational calibration update.

Fig. 5 compares *M*1 and *M*11 band-averaged *F*-factors and daily DCC time series during the PLT period. Both daily DCC and *F*-factors' time series were normalized to the first data point (January 6, 2018). It can be observed that daily DCC time series follow closely with *F*-factors. The calibration changes were detected successfully by the daily DCC time series. The visual examination of the daily DCC time series helps to detect a larger calibration change. For instance, *M*1 *F*-factor decreased by ∼4% on March 23, 2018, by the third update. Since the change is much larger than the noise level of the *M*1 daily DCC time series (∼1.1%), it was captured the next day on March 24, 2018. The small difference between the changes in *F*-factor and DCC reflectance is due to the noise in the daily DCC time series. Similarly, the calibration change in *M*11 caused by the second on-orbit calibration update (February 6, 2018, the first update for the SWIR bands) was also detected promptly on the next day.

The daily DCC method can also detect a persistent calibration change that is within the noise level. It usually requires a longer time and quantitative analysis to detect the smaller changes but still usually much faster than the monthly DCC method. Note that the daily DCC time series are noisy. It is very challenging, if not impossible, to explain the smaller changes in DCC reflectance for a single day. It is recommended to use statistics based on as much data as possible for more reliable results, especially for smaller calibration changes.

V. NOAA-20 VIIRS RSB Early On-Orbit Performance

NOAA-20 VIIRS achieved validate maturity status on April 30, 2018, after the latest calibration update on April 27, 2018. About 20 months of VIIRS RSB operational SDRs calibrated using constant *F*-Factors are available by the beginning of 2020. To obtain more reliable trending results, we reprocessed NOAA-20 SDRs during the early mission using the constant *F*-factors and demonstrated that more reliable results for the NOAA-20 RSB early on-orbit responsivity trends could be achieved. In this section, consolidated NOAA-20 SDRs (reprocessed: January 6, 2018–April 30, 2018, operational: May 1, 2018–January 5, 2020) were used to estimate instrument responsivity change over time. S-NPP daily DCC time series, generated using operational SDRs, during the same two-year period were also analyzed for comparison purpose. The annual cycle correction was applied for all S-NPP and NOAA-20 RSBs. Although the two-year observations are still short for long-term trend analysis, the results from this study may provide useful information about NOAA-20 RSB early on-orbit performance.

Note that applying the annual cycle climatology derived using the reprocess S-NPP data to the NOAA-20 DCC time series will not introduce spurious trends in the results. The annual cycles for NOAA-20 and S-NPP DCC time series are expected to be very close to each other. Moreover, the exact two years of time series were analyzed to characterize NOAA-20 RSB degradation trends in this study; therefore, the trend of the annual cycle correction term is zero. However, the annual cycle correction reduces the uncertainty of the trend. Moreover, the annual cycle correction will also not affect the interchannel and intersatellite biases because annual cycles in the bands to be compared are similar and will be canceled out in the band ratio time series.

A. NOAA-20 RSB On-Orbit Responsivity Trends

Fig. 6 shows NOAA-20 (top, consolidated) and S-NPP (bottom, operational) daily DCC time series for representative VIS/NIR bands. The two-year trends and 95% CI intervals for all bands are summarized in Table IV. All statistics were estimated after the annual cycle correction. It can be observed

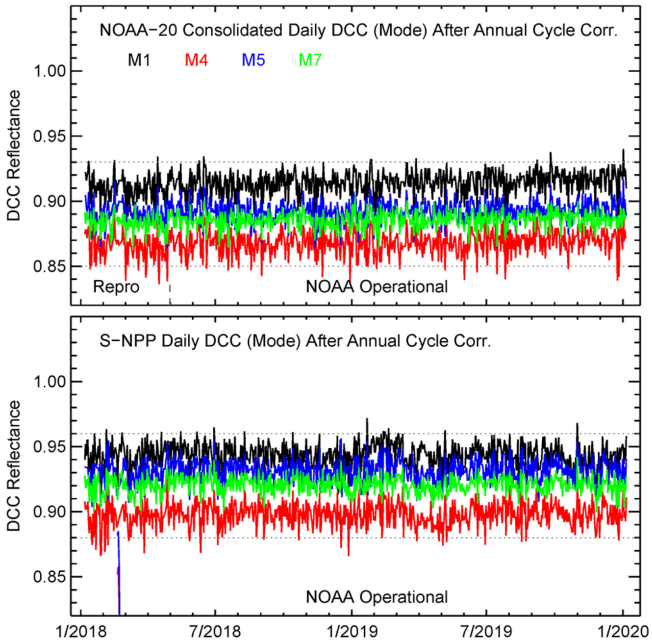

Fig. 6. Two-year daily DCC time series (January 6, 2018–January 5, 2020) for NOAA-20 (top, consolidated) and S-NPP (operational) bands *M*1, *M*4, *M*5, and *M*7.

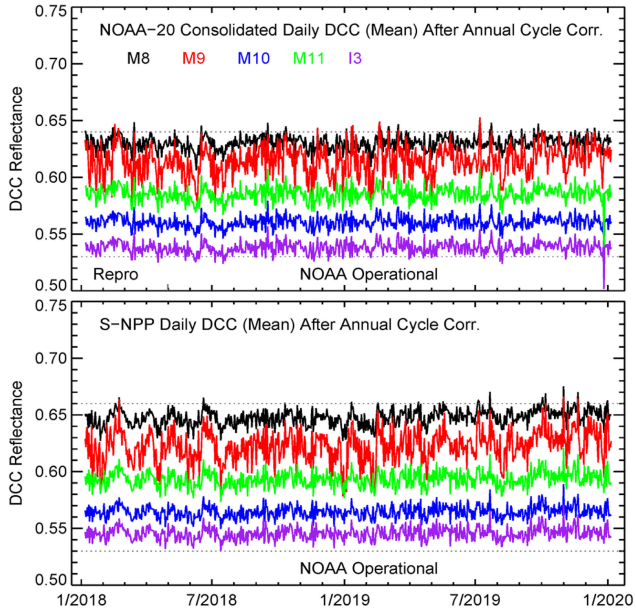

Fig. 7. Two-year daily DCC time series (January 6, 2018–January 5, 2020) for NOAA-20 (top, consolidated) and S-NPP (operational) SWIR bands.

TABLE IV
TWO-YEAR TRENDS (%/YEAR) AND 95% CONFIDENCE INTERVALS (CI) DERIVED USING NOAA-20 (CONSOLIDATED, REPROCESSED + OPERATIONAL) AND S-NPP (OPERATIONAL) RSB DAILY AND MONTHLY DCC TIME SERIES (JANUARY 6, 2018, TO JANUARY 5, 2020)

	Trend±95%CI	NOAA-20 (Consolidated)	S-NPP (Operational)
VIS/NIR	M1	0.4±0.1	-0.1±0.1
	M2	0.2±0.1	-0.1±0.1
	M3	0.3±0.1	0.1±0.1
	M4	0.3±0.1	0.1±0.1
	M5	0.2±0.1	0.1±0.1
	M7	0.2±0.1	-0.0±0.1
	I1	0.2±0.1	-0.0±0.1
	I2	0.2±0.1	-0.0±0.1
SWIR	M8	0.2±0.1	0.6±0.1
	M9	0.6±0.3	0.9±0.3
	M10	0.3±0.3	0.5±0.3
	M11	0.2±0.3	0.5±0.3
	I3	0.3±0.3	0.5±0.3

that the calibration jumps during the NOAA-20 early mission have been successfully addressed by the reprocessing (see Figs. 3 and 6). For S-NPP, the *M*4 and *M*5 calibrations anomaly (up to 20%, February 19–25, 2018) was successfully detected by the daily DCC method and not used for trend analysis. The S-NPP calibration anomaly from February 2019 to March 2019 was also captured by the daily DCC time series. Our analysis shows that this anomaly has no significant impact on the trends.

The consolidated daily DCC time series indicate that there is no large change in the NOAA-20 NIR responsivity after two years on-orbit, different from S-NPP that exhibits the significant degradations of up to 30% in the NIR spectrum during its early mission [2]. However, small upward trends were observed in the NOAA-20 daily DCC time series ranging from 0.2%/year to 0.4%/year. Moreover, 95% CIs indicate that these upward trends are significant. *M*1 exhibits the largest trend among all VIS/NIR bands, ∼0.4%/year (∼0.8% in two years), followed by *M*3 and *M*4 (∼0.3%/year). The trends in other VIS/NIR bands are ∼0.2%/year. The two-year trends derived in this section are similar to those derived using 1.5 years of daily DCC time series (see Table III, after the annual cycle correction) but with smaller uncertainty.

The DCC results are generally consistent with NOAA-20 solar *F*-factors (not used in the operational processing), which show small downward trends but with similar magnitudes as the daily DCC time series (NOAA STAR VIIRS SDR team, personal communication). In other words, both the DCC method and the solar calibration results indicate that the responsivity of NOAA-20 VIS/NIR bands, especially the shorter wavelength bands (*M*1–*M*4), may have been increasing slowly since launch. On the contrary, trends in the S-NPP daily DCC times are small, within ±0.1% for all VIS/NIR bands and similar to the uncertainty level. The on-orbit calibration of NOAA-20 VIS/NIR bands may need to be updated in the future.

Fig. 7 compares the daily DCC time series for NOAA-20 (top, consolidated) and S-NPP (bottom, operational) SWIR bands. Two-year trends are also summarized in Table IV. Similar to the VIS/NIR bands, NOAA-20 SWIR calibration jumps in the early mission were also successfully resolved after the reprocessing (see Figs. 4 and 7). The constant *F*-factors generally work well for the NOAA-20 SWIR bands.

Similar to the NOAA-20 VIS/NIR bands, the small upward trends were also observed in the NOAA-20 SWIR bands. The trend in *M*8 is significant and similar to that of *M*7. *M*9 shows a relatively larger trend (0.6%±0.3%) and the trend is significantly based on its 95% CI. The trends in *M*10 and *M*11 and *I*3 are similar to the uncertainty.

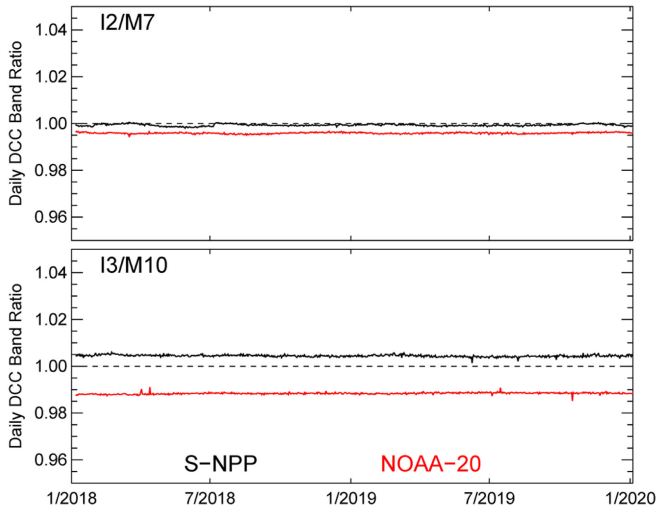

Fig. 8. *I2*/*M7* (top) and *I3*/*M10* (bottom) daily DCC band ratio time series for NOAA-20 and S-NPP.

The S-NPP SWIR bands exhibit larger upward trends than the NOAA-20 with trends ranging from 0.5%/year–0.9%/year, while the uncertainties are similar to NOAA-20. The trends in all four bands are significantly based on their 95% CIs. For S-NPP, SD degradation is not considered in the SWIR calibration, while it is accounted for in the VIS/NIR calibration. In addition, S-NPP SD counts, therefore *F*-factors, increased by ∼0.5% since February 24, 2019 (STAR VIIRS SDR Team, personal communication). This change was accounted for in the VIS/NIR bands by the RSBAutoCal SD degradation factor updates, but it is not addressed in the SWIR calibration. These factors may contribute to the larger upward trends observed in the S-NPP SWIR bands.

B. I2/M7 and I3/M10 Interchannel Calibration Consistency

We also evaluated NOAA-20 RSB interchannel calibration consistency using daily DCC ratio time series. VIIRS *I*-bands *I*2 and *I*3 have nearly identical center wavelengths with *M*-bands *M*7 and *M*10, respectively (see Table I). Fig. 8 shows the *I2*/*M7* and *I3*/*M10* band ratio time series for NOAA-20 and S-NPP. It can be seen that NOAA-20 *I*2 and *I*3 are less consistent with their *M*-bands' counterparts. *I*2 and *M*7 agree within 0.1% (S-NPP) and 0.4% (NOAA-20). S-NPP *I*3 calibration is generally consistent with *M*10 with a difference of ∼0.4%. However, the DCC band ratio time series indicate that larger discrepancy exists between NOAA-20 *I*3 and *M*10 with a difference of ∼1.2%. The root cause of the larger differences in NOAA-20 needs to be studied in the future.

C. NOAA-20 and S-NPP Intersatellite Biases

NOAA-20 and S-NPP RSB intersatellite biases were also evaluated using daily DCC ratios. The results are summarized in Table V. Fig. 9 shows the examples of NOAA-20 and S-NPP daily DCC reflectance ratios for bands *M*1, *M*4, *M*5, and *M*7. The spectral response differences between the two VIIRS

TABLE V
NOAA-20/S-NPP INTERSATELLITE BIASES ESTIMATED USING DAILY DCC BAND RATIOS AND OVER THE DOME-C AND LIBYAN4 VALIDATION SITES

Bias (%)		Daily DCC	Dome-C	Libyan4
VIS/NIR	M1	-3.4	-2.3	-2.2
	M2	-1.2	-1.1	-1.8
	M3	-2.6	-1.8	-3.8
	M4	-2.8	-2.3	-1.6
	M5	-4.3	-3.9	-3.2
	M7	-3.6	-3.4	-3.0
	I1	-3.1	-2.3	-2.2
	I2	-3.9	-3.3	-3.2
SWIR	M8	-2.6	-2.8	-2.2
	M9	-1.5	-	-
	M10	-3.1	-	-1.5
	M11	-2.3	-	-0.6
	I3	-4.1	-	-4.0

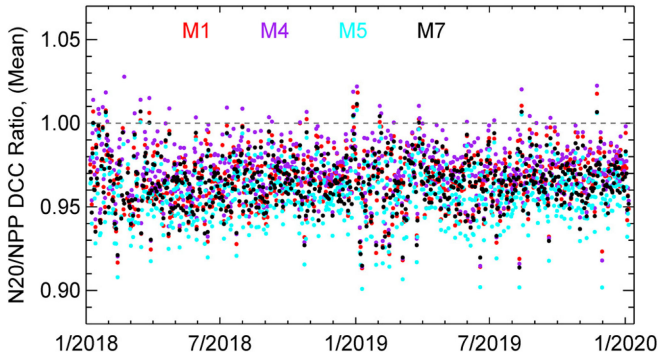

Fig. 9. NOAA-20 (consolidated) and S-NPP daily DCC ratios for bands *M*1, *M*4, *M*5, and *M*7.

were estimated and corrected using the SCIAMACHY-based SBAFs (see Section III-A). The SBAFs over DCCs are within 0.6% for VIS/NIR bands and 1.3% for SWIR bands. After the SBAF correction, NOAA-20 RSBs bias about 1.5%–4.5% lower relative to S-NPP. *M*1, *M*5, *M*7, *M*10, and *I*1–*I*3 show larger intersatellite biases, more than 3%. Moreover, NOAA-20/S-NPP RSB biases become smaller over time, which may be due to the gradual increase of NOAA-20 instrument response over time (see Section V-A and Fig. 9).

We compared NOAA-20/S-NPP intersatellite biases derived using the daily DCC method with other methods. Similar biases were observed in the monthly DCC ratios. The daily DCC ratios derived biases agree with those estimated using NOAA-20/MODIS-Aqua and S-NPP/MODIS-Aqua SNO time series within 1% for most of the bands (NOAA STAR VIIRS SDR team, personal communication). The DCC method derived biases also generally agree with those estimated using the validation site time series over Dome-C and Libyan4 desert [19]. NOAA-20/S-NPP biases estimated over the two vicarious sites using nadir clear-sky observations from May 1, 2018, to January 5, 2020, are also given in Table V. Fig. 10 shows an example of NOAA-20 and S-NPP *M*5 top-of-atmosphere reflectance time series over Libyan4. The spectral differences between NOAA-20 and S-NPP over the two sites were corrected

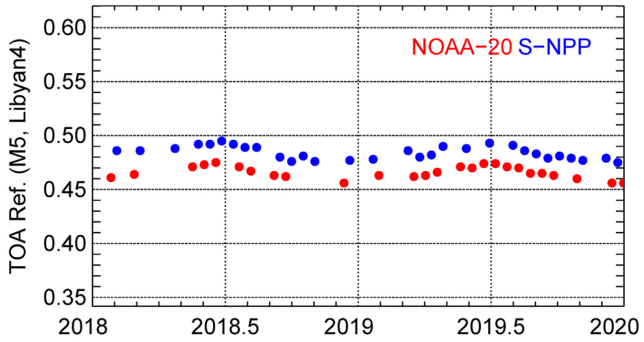

Fig. 10. NOAA-20 (red) and S-NPP (blue) band *M*5 TOA reflectance time series over the Libyan4 desert site.

using the SCIAMACHY-based SBAFs (see Section III-A). Note that there are no sufficient data for bands *M*9–*M*11 and *I*3 over the Dome-C site and band *M*9 over the Libyan4 site. The biases in these bands were not estimated. The biases estimated over the two validation sites also agree (within 1.0% for most of the bands) with those estimated using the daily DCC method. More studies are currently ongoing to investigate the root cause of NOAA-20/S-NPP RSB biases.

VI. Summary

This study evaluates NOAA-20 VIIRS RSB early on-orbit performance using the daily DCC method. A DCC annual cycle climatology was developed with four years of S-NPP reprocessed data and was used to correct residual annual variations in the DCC time series for NOAA-20 and S-NPP. Therefore, more reliable trends can be derived using relatively short data records. Although daily DCC time series are noisier, the trends derived using this method are consistent with those of the monthly DCC method (within $\pm$0.1%/year). Moreover, the uncertainty of trends derived using the daily method is smaller due to the larger number of data points in the time series. We have also compared NOAA-20 daily DCC time series with on-orbit *F*-factor changes during the PLT period. Our results indicate that the daily DCC time series can provide timely information about on-orbit calibration changes. It is valuable to support decision making of the VIIRS RSB operational update during the PLT when other vicarious methods are not applicable. It is also useful to detect the short-term calibration anomalies that are usually overlooked by the monthly DCC method.

NOAA-20 VIIRS RSB SDRs have been calibrated using constant *F*-factors since April 27, 2018, with the assumption that no on-orbit instrument responsivity change occurred. In this study, we reprocessed NOAA-20 VIIRS SDRs during the early mission using consistent, constant *F*-factors. Two-year trends were analyzed using the consolidated daily DCC time series and compared with S-NPP. The improved results show that NOAA-20 VIS/NIR bands detector responses may have increased slowly over time with trends ranging from 0.2%/year to 0.4%/year and above the uncertainty level. *M*1 exhibits the largest upward trend (0.4%/year). Future calibration updates may be required to address this issue.

We have also evaluated the NOAA-20 interchannel calibration consistency and NOAA-20/S-NPP intersatellite biases using daily DCC ratios. The results show that NOAA-20 *I*3 and *M*10 are less consistent with each other with a difference of $\sim$1.2%. NOAA-20 RSBs bias $\sim$1.5%–4.5% lower than S-NPP. The biases larger than 3% were observed in *M*1, *M*5, *M*7, and *I*1–*I*3. The intersatellite biases derived using the daily DCC method are generally consistent with the results estimated using other methods. The results of this study will provide useful information to the NOAA-20 and S-NPP VIIRS SDR user community. The methodology presented in this article can also be applied to the VIIRS onboard the future JPSS satellites and other radiometers.

Acknowledgment

The views, opinions, and findings contained in this article are those of the authors and should not be construed as an official NOAA or the U.S. Government position, policy, or decision. The authors would also like to thank Dr. Slawomir Blonski and Dr. Taeyound Choi from the NOAA STAR VIIRS SDR team for their valuable suggestions and comments.

References

[1] C. Cao *et al.*, "Suomi NPP VIIRS sensor data record verification, validation, and long-term performance monitoring," *J. Geophys. Res., Atmos.*, vol. 118, no. 20, pp. 11664–11678, 2013.

[2] C. Cao, F. J. De Luccia, X. Xiong, R. Wolfe, and F. Weng, "Early on-orbit performance of the visible infrared imaging radiometer suite onboard the suomi national polar-orbiting partnership (S-NPP) satellite," *IEEE Trans. Geosci. Remote Sens.*, vol. 52, no. 2, pp. 1142–1156, Feb. 2014.

[3] C. Cao *et al.*, "NOAA-20 VIIRS on-orbit performance, data quality, and operational cal/val support," presented at the SPIE Asia-Pac. Remote Sens., Honolulu, HI, USA, p. 107810K, 2018.

[4] D. R. Doelling, D. Morstad, B. R. Scarino, R. Bhatt, and A. Gopalan, "The characterization of deep convective clouds as an invariant calibration target and as a visible calibration technique," *IEEE Trans. Geosci. Remote Sens.*, vol. 51, no. 3, pp. 1147–1159, Mar. 2013.

[5] Y. Hu, B. A. Wielicki, P. Yang, P. W. Stackhouse, B. Lin, and D. F. Young, "Application of deep convective cloud albedo observation to satellite-based study of the terrestrial atmosphere: Monitoring the stability of spaceborne measurements and assessing absorption anomaly," *IEEE Trans. Geosci. Remote Sens.*, vol. 42, no. 11, pp. 2594–2599, Nov. 2004.

[6] R. Bhatt *et al.*, "Initial stability assessment of S-NPP VIIRS reflective solar band calibration using invariant desert and deep convective cloud targets," *Remote Sens.*, vol. 6, no. 4, pp. 2809–2826, 2014.

[7] W. Wang and C. Cao, "DCC radiometric sensitivity to spatial resolution, cluster size, and LWIR calibration bias based on VIIRS observations," *J. Atmos. Ocean. Technol.*, vol. 32, no. 1, pp. 48–60, Jan. 2015.

[8] W. Wang and C. Cao, "Monitoring the NOAA operational VIIRS RSB and DNB calibration stability using monthly and semi-monthly deep convective clouds time series," *Remote Sens.*, vol. 8, no. 1, 2016, Art. no. 32.

[9] W. Wang, "Daily DCC ratio time series: NOAA-20 versus S-NPP," presented at the VIIRS SDR Team Weekly Telecon, College Park, MD, USA, 2018.

[10] W. Wang and C. Cao, "NOAA-20 VIIRS sensor data records geometric and radiometric calibration performance one year in-orbit," in *Proc. IEEE Int. Geosci. Remote Sens. Symp.*, Yokohama, Japan, 2019, pp. 8485–8488.

[11] X. Gong, Z. Li, J. Li, C. C. Moeller, and W. Wang, "Monitoring the VIIRS sensor data records reflective solar band calibrations using DCC with collocated CrIS measurements," *J. Geophys. Res., Atmos.*, vol. 124, no. 15, pp. 8688–8706, Aug. 2019.

[12] S. Blonski and C. Cao, "Suomi NPP VIIRS reflective solar bands operational calibration reprocessing," *Remote Sens.*, vol. 7, no. 12, pp. 16131–16149, 2015.

[13] K. Rausch, S. Houchin, J. Cardema, G. Moy, E. Haas, and F. J. De Luccia, "Automated calibration of the Suomi national polar-orbiting partnership (S-NPP) visible infrared imaging radiometer suite (VIIRS) reflective solar bands," *J. Geophys. Res., Atmos.*, vol. 118, no. 24, pp. 13434–13442, 2013.
[14] NOAA STAR, "S-NPP VIIRS version 2 reprocessed sensor data records." [Online]. Available: https://ncc.nesdis.noaa.gov/VIIRS/index.php, Accessed: Feb. 28, 2020.
[15] R. Bhatt, R. D. Doelling, B. Scarino, C. Haney, and A. Gopalan, "Development of seasonal BRDF models to extend the use of deep convective clouds as invariant targets for satellite SWIR-band calibration," *Remote Sens.*, vol. 9, no. 10, 2017, Art. no. 1061.
[16] B. R. Scarino *et al.*, "A web-based tool for calculating spectral band difference adjustment factors derived from SCIAMACHY hyperspectral data," *IEEE Trans. Geosci. Remote Sens.*, vol. 54, no. 5, pp. 2529–2542, May 2016.
[17] H. Bovensmann *et al.*, "SCIAMACHY: Mission objectives and measurement modes," *J. Atmos. Sci.*, vol. 56, no. 2, pp. 127–150, Jan. 1999.
[18] D. C. Montgomery and G. C. Runger, *Applied Statistics and Probability for Engineers*, 7th ed. New York, NY, USA: Wiley, 2018.
[19] W. Wang, "SNPP VIIRS validation site time series." [Online]. Available: http://ncc.nesdis.noaa.gov/VIIRS/VSTS.php, Accessed: Oct. 30, 2015.

Wenhui Wang received the B.S. and M.S. degrees in computer science from Xi'an Jiaotong University, Xi'an, China, in 1991 and 1994, respectively, and the Ph.D. degree in geography specializing in remote sensing from the University of Maryland, College Park, MD, USA, in 2008.

She is currently a Visiting Associate Research Scientist with the CISESS/University of Maryland, College Park, MD, USA. From 2018 to 2019, she was a Senior Scientist with the Global Science and Technology, Inc. From 2013 to 2018, she was a Senior Scientist with the Earth Resources Technology, Inc. From 2008 to 2013, she was a Support Scientist with I. M. Systems Group, Inc. From 1994 to 2001, she was a Senior Software Engineer with the Institute of Computing Technology, Chinese Academy of Science, Beijing, China. Her research interests include satellite instrument calibration and validation, climate data records, surface radiation budget, and geovisualization.

Changyong Cao received the B.S. degree of Science in geography from Peking University, Beijing, China, in 1982, and the Ph.D. degree in geography specializing in remote sensing from Louisiana State University, Baton Rouge, LA, USA, in 1992.

He is a Research Physical Scientist with the NOAA/NESDIS/Center for Satellite Applications and Research. He specializes in the calibration of radiometers onboard NOAA's Operational Environmental Satellites and currently leads the VIIRS sensor science team. He has made significant contributions to the international and interagency satellite instrument calibration/validation community, including the Committee on Earth Observation Satellites and World Meteorological Organization Global Space-Based Intercalibration System. Before joining NOAA, in 1999, he was a Senior Scientist with five years of aerospace industry experience supporting NASA projects.

Dr. Cao was a recipient of two gold and one silver medal honored by the U.S. Department of Commerce for his scientific and professional achievements.